Journal of Materials Chemistry A

ROYAL SOCIETY OF CHEMISTRY

COMMUNICATION

View Article Online
View Journal

Cite this: DOI: 10.1039/d4ta03879g

Received 4th June 2024
Accepted 15th August 2024

DOI: 10.1039/d4ta03879g

rsc.li/materials-a

Exploring *ortho*-dianthrylbenzenes for molecular solar thermal energy storage†

Nicolò Baggi, [ab] Lidiya M. Muhammad, [c] Zacharias Liasi, [d] Jacob Lynge Elholm, [b] Paulius Baronas, [b] Elies Molins, [a] Kurt V. Mikkelsen [d] and Kasper Moth-Poulsen *[abce]

Molecular solar thermal systems, which absorb light, store it, and release it as heat, have been extensively researched, yet many potential candidates remain unexplored. To expand this range, five specifically designed *ortho*-dianthrylbenzenes were investigated. Anthracene dimers have been underexplored due to issues like photooxidation and varying photodimerization efficiency. The presented systems address these challenges by aryl-linking two anthracene moieties, achieving photodimerization quantum yields ranging from 11.5% to 16% in mesitylene. The impact of donor or acceptor groups on energy storage time (9–37 years), energy storage density (0.14–0.2 MJ kg^{-1}), and solar energy storage efficiency (0.38–0.66%) was evaluated. The experimental results, supported by density functional theory-based modeling, highlight the potential of anthracene-based photoswitches for molecular solar thermal applications and encourage further exploration of similar systems.

Introduction

Driven by the need to address the escalating global energy consumption, molecular solar thermal (MOST) systems are emerging as a promising renewable energy storage concept.[1–11] MOST systems are based on molecular photochromes capable of absorbing sunlight, storing it, and releasing it on-demand as thermal energy in a closed cycle. The four most studied[12] photoswitches for this application are azobenzenes,[13,14] norbornadiene–quadricyclane (NBD-QC) couples,[15,16] dihydroazulenes–vinylheptafulvenes,[17–19] and (fulvalene)tetracarbonyl-diruthenium derivatives.[20]

Anthracene dimers were first proposed for solar energy storage in 1909,[21] and the photo-induced dimerization of anthracene has been extensively analyzed.[22–28] However, while their potential use as solid-state MOST systems has been recently demonstrated by Han and co-workers,[29] no systematic study has been conducted on their application in solution in solar energy storage, to the best of our knowledge. Despite their promising absorption in the violet portion of the visible spectrum, several factors have limited the exploration of these derivatives for this application. These include the degradation of anthracene monomers upon photooxidation in solution[30] and their concentration-dependent photodimerization quantum yield.[31]

Generally, both challenges can be mitigated in solid-state switching, as described for multiple anthracene monomers either in single crystals[22,32–34] or in anthracene-containing polymers.[35–39] The latter issue can be resolved in solution by linking two anthracene moieties within a single molecule.[40,41] This linkage can also increase bond strain in the photodimer, thereby enhancing the energy storage density. While most examples in the literature focus on alkyl-linked anthracenes (*e.g.* di(9-anthryl)methane by Bergmark *et al.*),[23] the use of aromatic linkers has only been recently explored.[42–45]

Inspired by the work on 1,2-di(9-anthryl)benzene (**1o** in Fig. 1) by Nishiuchi, Kubo and co-workers,[42] who first reported the photoisomerization of this molecule and determined the storage energy ($\Delta G_{storage}$) and the storage energy density ($\rho_{storage}$) in its "closed" photoisomer, **1c** (*i.e.* $\Delta G_{storage}$ = 22.8 kcal mol^{-1} = 95.4 kJ mol^{-1} and $\rho_{storage}$ = 0.222 MJ kg^{-1}, that is higher than or comparable to the ΔH of other reported anthracene systems[23,41,42] and other MOST candidates[7]), we develop here the series of *ortho*-dianthryl-based photoswitches (**1o–5o**) depicted in Fig. 1. In these compounds, the phenyl linker is functionalized with electron-donating or electron-withdrawing groups.

Herein, we present a study of the properties of **1o–5o** for potential MOST applications, with a focus on the influence of

[a]The Institute of Materials Science of Barcelona, ICMAB-CSIC, Bellaterra, 08193 Barcelona, Spain. E-mail: kasper.moth-poulsen@upc.edu
[b]Department of Chemical Engineering, Universitat Politècnica de Catalunya, EEBE EduardMaristany 10-14, 08019 Barcelona, Spain
[c]Department of Chemistry and Chemical Engineering, Chalmers University of Technology, SE-41296 Gothenburg, Sweden
[d]Department of Chemistry, University of Copenhagen, Universitetsparken 5, Copenhagen Ø 2100, Denmark
[e]Catalan Institution for Research & Advanced Studies, ICREA, Pg. Lluís Companys 23, 08010 Barcelona, Spain

† Electronic supplementary information (ESI) available. CCDC 2359711–2359712. For ESI and crystallographic data in CIF or other electronic format see DOI: https://doi.org/10.1039/d4ta03879g

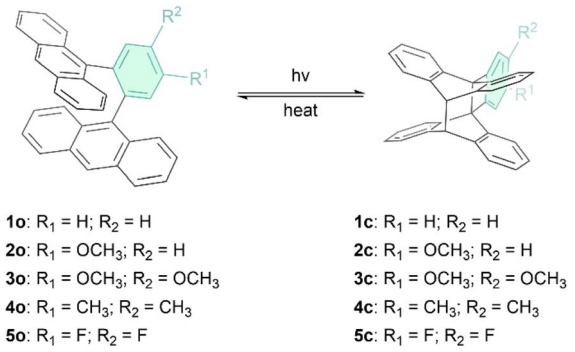

Fig. 1 The two states of the five investigated *ortho*-dianthrylbenzenes (**1o–5o**), where "o" denotes the open form and "c" denotes the corresponding closed photoisomers (**1c–5c**).

substitutions on the aryl bridge on energy storage time, solar spectrum match and energy storage density. The experimental work is complemented by theoretical modelling to rationalize the experimental observations.

Results and discussion

Compounds **1o–5o** were synthesized *via* Suzuki–Miyaura cross-coupling between 9-anthraceneboronic acid pinacol ester (instead of 9-anthraceneboronic acid, as previously reported in the literature[42,46]) and the corresponding di-halogenated phenyl rings. The detailed experimental procedures and the full characterization of the switches by NMR spectroscopy and high-resolution mass spectrometry (HRMS) are provided in the ESI† (Section "Synthetic procedures"). Among these derivatives, dianthracene **3o**, featuring a 4,5-dimethoxy-phenyl linker, had been previously synthesized through Negishi coupling, but no characterization for solar thermal energy storage was reported.[47] Overall, the *ortho*-dianthrylbenzenes molecules were obtained in yields ranging from 15% to 53%, with higher yields achieved when the product was isolated by recrystallization rather than column chromatography. We speculate that the limited solubility of the molecules may lead to product loss during chromatography, either because of strong adsorption to silica or precipitation from the solution. It is worth noting that **3o** was obtained in 68% yield (over two steps) *via* Negishi coupling,[47] thus indicating that such a synthetic route could be more effective for this class of derivatives.

The synthesized *ortho*-dianthrylbenzenes were investigated in non-degassed mesitylene at room temperature. The recorded UV-vis spectra were comparable across the series (Fig. S1†), displaying the distinctive bands of the anthracene moiety (Fig. 2). For instance, the absorption of *ortho*-xylene-linked **4o** starts at approximately 430 nm and peaks around 370 nm. Spectroscopic data including the maximum absorption wavelength (λ_{max}), molar absorption coefficient (ε) and onset wavelength (λ_{onset}) are listed in Table 1.

While λ_{max} and λ_{onset} were unaffected by the introduction of functional groups, the presence of electron-donating groups (*e.g.* $-OCH_3$ in **2o** and **3o**, and $-CH_3$ in **4o**) resulted in a higher ε compared to that of **1o**. Conversely, the electron-poorer

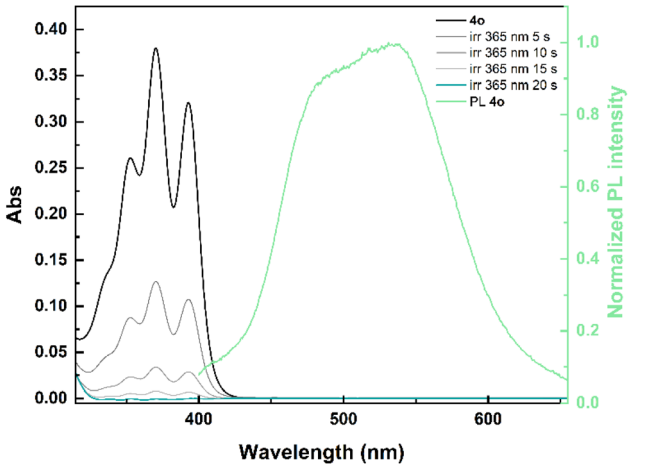

Fig. 2 Spectral evolution of **4o** (2.2×10^{-5} M, black solid line) in mesitylene under light irradiation (365 nm) at room temperature to **4c** (blue-green solid line) and normalized emission (clear green solid line) of **4o** in mesitylene upon excitation at 365 nm.

Table 1 Main optical data of the investigated photoswitches **1o–5o** in mesitylene

	λ_{max} (nm) [ε (10^3 M^{-1} cm^{-1})]	λ_{onset}[a] (nm)	Φ_{o-c} (%)	Φ_F (%)
1o	372 [15.6]	425	16	1.8
2o	372 [16.4]	426	13	1.7
3o	373 [17.1]	425	11.5	2.9
4o	372 [17]	424	13	2.2
5o	372 [14.9]	426	16	1.7

[a] λ_{onset}: $\log(\varepsilon) = 2$.

dianthrylbenzene **5o** exhibited the lowest molar extinction coefficient within the series.

Switches **1o–5o** are also fluorescent, albeit with low quantum yields (<3%). The emission is observed between approximately 390 nm and 725 nm (emission spectrum of **4o** in Fig. 2, emission spectra of **1o–3o** and **5o** in Fig. S2†). This emission is attributed to a combination of the photoluminescence of anthracene and an intramolecular excimer formation.

Upon irradiation at 365 nm, all photoswitches underwent rapid isomerization (Fig. 2 and S1†) to their corresponding photoisomers **1c–5c**, with a concurrent fluorescence quenching as these adducts are non-emissive due to the loss of anthracene conjugation.[42] Moreover, a large optical contrast can be observed between **1o–5o** and **1c–5c** since the latter have only negligible absorption between 300 nm and 425 nm.

To assess if the isomerization could be achieved in real solar conditions, a solution of **4o** in non-degassed mesitylene was exposed to unfiltered sunlight. The recorded spectra showed also in this case a fast isomerization to **4c** (Fig. 3), with no degradation. Considering the comparable optical properties of **1o–3o** and **5o**, a similar behaviour can be expected also for the other investigated photoswitches.

Both the isomerization (Φo–c) and the fluorescence (Φ_F) quantum yields were determined in mesitylene and are summarized in Table 1.

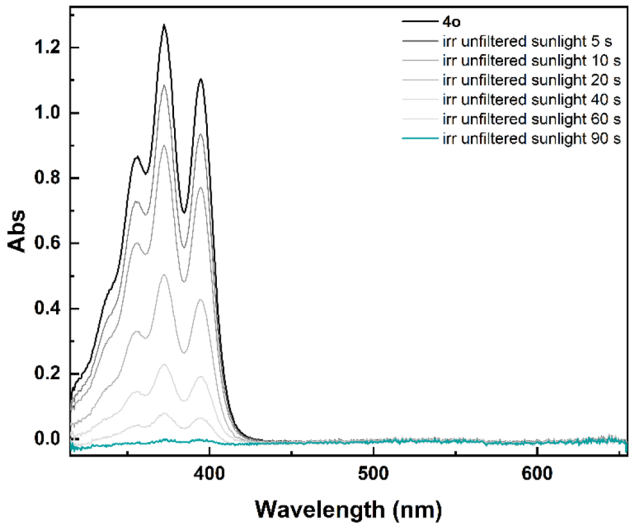

Fig. 3 Spectral evolution of **4o** (7.5×10^{-5} M) to **4c** in mesitylene under unfiltered sunlight irradiation.

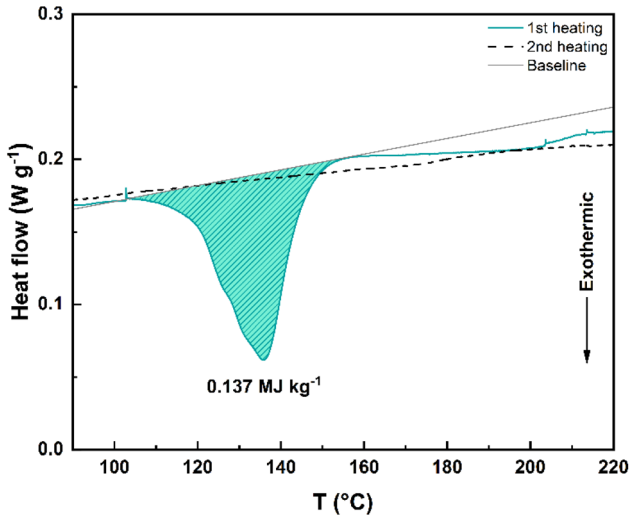

Fig. 4 DSC graph of **4c** showing the heat release during the first heating cycle (blue-green solid line). No heat release was observed during the second heating cycle (black dashed line). The baseline used for the integration to determine the energy release is provided with a solid grey line for clarity.

Φo–c values around 16% were measured for **1o** and **5o**. In contrast, the three switches bearing donor groups showed lower efficiencies, particularly **3o**, with an isomerization quantum yield of 11.5%. These values are comparable to those reported for certain anthracene monomers – where concentration is also a critical factor – and other linked systems.[23,25,26]

Additionally, photo-induced isomerization and fluorescence are two competitive excited-state processes. The fluorescence quantum yield of **3o** is the highest within the series (2.9%), while Φ_F of the other studied molecules range from 1.7 to 1.8% for **2o**, **5o** and **1o**, and is equal to 2.2% for **4o**. In general, these values appear lower than those of anthracene or other monomers, likely due to the increased strain in the aryl-linked systems. Details on the determination of Φo–c and Φ_F are provided in the ESI† (Sections "Determination of the photoisomerization quantum yields" and "Determination of the fluorescence quantum yields" of the ESI†, respectively).

Next, the thermal stability of **1c–5c**, photogenerated in mesitylene, was studied through differential scanning calorimetry (DSC). The DSC graph of **4c** is depicted in Fig. 4 and it shows the exothermic process (only during the first heating cycle, starting at around 100 °C and ending around 155 °C) associated to the putative[42] stepwise bond dissociation that accompanies the back-reaction. The corresponding storage energy ($\Delta G_{storage}$) and storage energy density ($\rho_{storage}$) are 62.8 kJ mol^{-1} and 0.137 MJ kg^{-1}, respectively (Table 2). In the case of **5c**, the heat release occurs between 140 °C and 185 °C and an endothermic process (possibly **5c** melting) is observed between 80 °C and 100 °C *ca.* (Fig. S3d†).

However, the DSC experiments for **1c–3c** (Fig. S3a–c†) showed exothermic events that were difficult to interpret, perhaps due to interactions of the photoisomers with residual traces of mesitylene. Therefore, the dissociation of the C9–C9′ and the C10–C10′ single bonds in **1c–5c** to restore the parent molecules **1o–5o** was also studied on photoisomers prepared upon irradiation in DMSO (Fig. S4†). In this case, the obtained DSCs allowed the determination of the corresponding storage energies and storage energy densities (Table 2).

For comparison, the observed $\Delta G_{storage}$ for **1c**, **2c** and **3c** (86.1 kJ mol^{-1}, 94.0 kJ mol^{-1} and 69.2 kJ mol^{-1}, respectively) are higher than the $\Delta G_{storage}$ of anthracene (65.2 kJ mol^{-1})[41] and

Table 2 Thermodynamic data for thermal back-conversion (**1c–5c** → **1o–5o**) determined from the Eyring equation including the activation enthalpy (ΔH^*) and entropy (ΔS^*), and half-lives at 25 °C ($t_{1/2}$); storage energies ($\Delta G_{storage}$), storage energy densities ($\rho_{storage}$) and solar energy storage efficiencies (η_{MOST}). The theoretical values, computed at the ωB97X-D3(BJ)/cc-pVTZ level of theory, are given in square brackets for vacuum and *implicit mesitylene*, respectively

	ΔH^* (kJ mol^{-1})	ΔS^* (J K^{-1} mol^{-1})	$t_{1/2}$ (years)	$\Delta G_{storage}$ (kJ mol^{-1})	$\rho_{storage}$ (MJ kg^{-1})	η_{MOST} (%)
1	121	−7.6	15	86.1[b] [63.4, *62.4*]	0.200 [0.147, *0.145*]	0.66
2	127	8.8	25	94.0[b] [66.9, *63.7*]	0.204 [0.145, *0.138*]	0.58
3	125	3.8	18	69.2[b] [68.7, *67.7*]	0.141 [0.140, *0.138*]	0.38
4	122	−0.9	9	62.8[a]	0.137[a]	0.41
				65.6[b] [67.7, *66.0*]	0.143[b] [0.148, *0.144*]	
5	128	9.0	37	64.8[a]	0.139[a]	0.57
				74.6[b] [64.3, 63.5]	0.160[b] [0.138, *0.136*]	

[a] Prepared in mesitylene. [b] Prepared in DMSO.

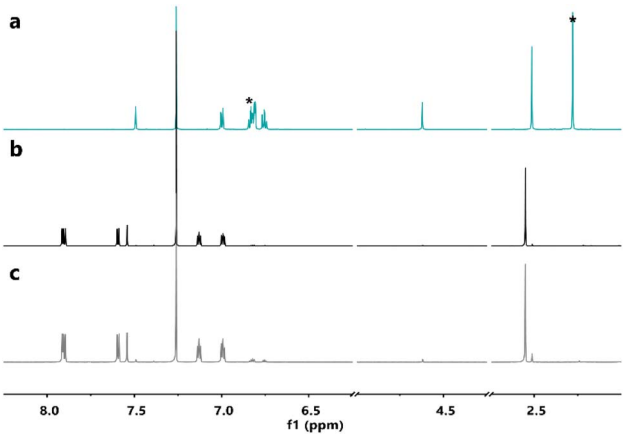

Fig. 5 ^{1}H-NMRs in $CDCl_3$ of (a, blue-green solid line) **4c** after irradiation at 365 nm in non-degassed mesitylene; (b, black solid line) **4o** before irradiation at 365 nm in non-degassed mesitylene; and (c, grey solid line) recovered **4o** after the DSC measurement. *: peaks of residual mesitylene.

other linked anthracene-based MOST candidates (*e.g.* $\Delta G_{storage}$ = 35.5 kJ mol^{-1} in the photoisomer of bi(anthracene-9,10-dimethylene)).[41]

The storage energy densities ($\rho_{storage}$) ranging from 0.14 MJ kg^{-1} to 0.2 MJ kg^{-1} within the series appear to be similar to those of some azobenzene-based molecular solar thermal systems or fulvalene-tetracarbonyl-diruthenium, but lower than that of norbornadiene–quadricyclane couples due to the higher molecular weight.[7]

Furthermore, ^{1}H-NMR spectroscopy of the samples after the DSC measurements indicated that the parent molecules could be recovered without degradation (Fig. 5, S5 and S6†), confirming a clean solid-state back-reaction.

The high temperatures required for back-conversion indicate that the photoisomers of the five investigated *ortho*-dianthrylbenzenes are not particularly thermally labile.

Kinetic studies in mesitylene ("Kinetic studies" section in the ESI†) were carried out to determine the half-lives of the photoisomers (Table 2), confirming that **1c–5c** are stable for several years at room temperature, suggesting their suitability for long-term energy storage. Notably, **2c** and **5c** appeared to be significantly more stable than reference **1c**, with half-life times of 25 years and 37 years at 25 °C, respectively, compared to 15 years, while the half-life of the *ortho*-xylene-linked **4c** dropped to 9 years.

Having determined all the required parameters, the solar energy storage efficiencies (η_{MOST}) of the investigated *ortho*-dianthrylbenzenes were calculated (Table 2 and "Solar energy storage efficiency" section in the ESI†) assuming no competitive absorption of the photoisomers **1c–5c** between 300 nm and λ_{onset} (UV-vis spectra in Fig. 2 and S1†). η_{MOST} ranging from 0.38% for **3** to 0.66% for **1** are on par with those of some azo-based MOST systems (0.11% to 0.43% for azobenzenes, 0.59% to 0.94% for azopyrazoles)[48] and norbornadiene-quadricyclane couples (0.51–0.7%),[7] although somewhat lower than the recent record solar capture efficiency for NBDs (2.3%).[49] Analysing eqn S2† ("Solar energy storage efficiency" section in the ESI†) in context of **1–5**, absorbance and onset of absorption are attractive properties of these systems, but the relatively low Φ_{o-c} (from 11.5% to 16%) are the main factor reducing solar capture efficiency, illustrating that future improvements in the photoisomerization quantum yield could significantly boost this parameter.

To complement the synthesis and experimental investigation of the considered *ortho*-dianthrylbenzenes, a computational investigation of the primary properties desired for a MOST system was also carried out. A GFN2-xTB-based[50] screening approach was used to identify the lowest-energy conformers. Subsequent geometry optimizations were performed using r^{2}SCAN-3c[51] and ωB97X-D3(BJ)[52] to determine the energy storage capacity of the given systems. The minima obtained using ωB97X-D3(BJ) were used for a climbing image nudged elastic band (CI-NEB) search,[53] utilizing GFN2-xTB, to identify the transition states. For the resulting transition states a frequency analysis using ωB97X-D3(BJ) was carried out. Additionally, absorption spectra were simulated for the open and closed states of the photoswitches to evaluate their overlap with the solar spectrum. The conformer search was conducted using an in-house script linked to the xtb program package (Release 6.7.0),[54] while all subsequent calculations were carried out in ORCA (Release 5.0.1).[55] This overall approach aligns with earlier work on other organic photoswitches for MOST applications[56–58] and is described in-depth in the ESI† ("Theoretical modelling details" section).

The experimental storage energies and related densities display significant variation in the energy storage capabilities of the selected systems under the employed conditions. Compared to the experimental values, the computed values in vacuum are generally lower, ranging from 63.4 kJ mol^{-1} to 68.7 kJ mol^{-1} (Table 2). This discrepancy can be attributed to the idealized conditions assumed in the calculations, which do not fully capture the complexity of the environment present in the experiments. This may also explain—at least partially—that the variation in the computed values is less pronounced than in the experimental ones. When implicit mesitylene is included, the computed values are slightly adjusted but still remain lower than the experimental values. The range in this case (63.4 kJ mol^{-1} to 67.7 kJ mol^{-1}) indicates a modest impact of the solvent environment on the computed Gibbs free storage energy. The solvent appears to slightly lower the energy values, particularly for the **2o** and **4o** systems.

The predicted energy barriers for both the initial switching and the back-conversion are higher than expected. They all lie relatively close to each other, with the predicted reaction barriers in the range of 304.4 to 312.7 kJ mol^{-1}, while the back-reaction barriers lie in the range of 241.0 to 245.0 kJ mol^{-1}, as presented in Table S1.† Although higher than expected, the predicted values align well with the DSC results, indicating a thermally stable set of photoswitches. This agreement extends to the measured kinetics, despite the lack of a pronounced discrepancy between the highest and lowest barriers.

As for the storage energies, the inclusion of implicit mesitylene only has a modest impact on the predicted values. Notably, according to the CI-NEB search, the switching

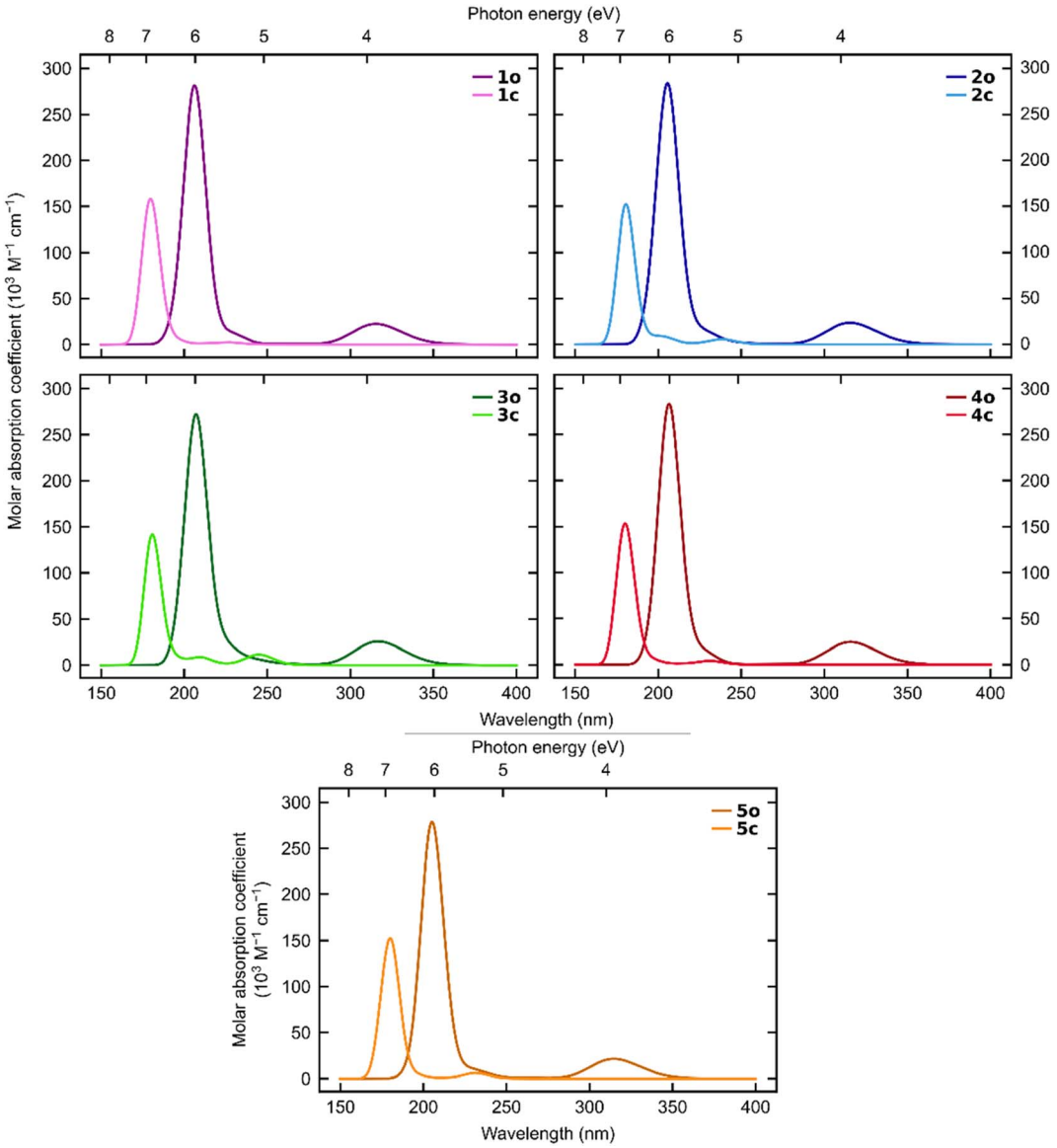

Fig. 6 Simulated absorption spectra for **1**–**5** at the ωB97X-D3(BJ)/aug-cc-pVDZ level of theory.

mechanism is stepwise regarding bond formation. Specifically, for each system, the transition is initiated by the formation of a bond between the two carbons directly connected to the linker, *i.e.*, a C9–C9′ single bond, as shown in Fig. S21 in the ESI.† This is consistent with the X-ray structures ("Crystal structure details" section in the ESI†), where the distance between those carbon atoms is around 3.06 Å, and the C10 and C10′ atoms are about 6.28–6.36 Å from each other. This

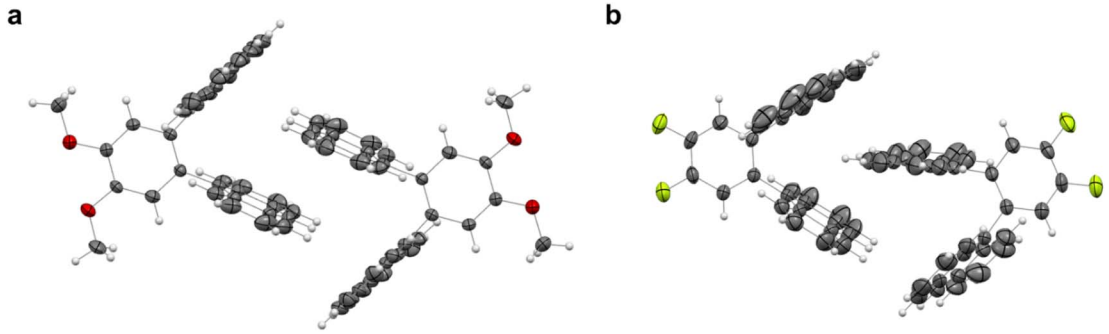

Fig. 7 Crystal structures of (a) **3o** and (b) **5o**. Thermal ellipsoids were set at the 30% probability level and bonds were depicted in wireframe style.

indicates that the transition state of each system can be characterized by the presence of only a single bond. The corresponding distances in the theoretical transition states are 1.70 to 1.71 Å for the C9–C9′ bond and 3.00 to 3.02 Å for the C10–C10′ bond, as presented in Table S2.† Although interesting, the stepwise transition from the open to closed state makes the transition state search significantly more challenging, as most attempts result in a minimum—if they converge.

The simulated UV-vis spectra (Fig. 6) show a clear separation between the open and closed states regarding absorption of visible light for all five systems.

Although both states absorb light below 270 nm, only the open states absorb at longer wavelengths. This demonstrates that all five *ortho*-dianthrylbenzenes are theoretically capable of absorbing sunlight and then storing it without undergoing a competitive photo-induced back-reaction. This finding aligns with the experimentally observed behaviour. This is a desirable trait for a potential MOST system, and in combination with the relatively high storage capacity, indicates that further investigation of anthracene-based photoswitches for MOST applications may be worthwhile.

Aiming to investigate any possible photo-induced isomerization in a condensed state, single crystals of **3o** and **5o** were grown through liquid–liquid diffusion in dichloromethane and methanol ("Crystal structure details" section in the ESI†). As reported in the literature for **1o**, no formation of **3c** and **5c** was observed upon light irradiation.

This can be ascribed to the steric hindrance caused by the molecules' packing in the crystals (Fig. 7a and b). Indeed, the V-shaped *ortho*-dianthrylbenzenes appear to be intertwined because of the existing van der Waals forces between the anthracene moieties of two neighbour molecules, thus probably inhibiting any possible isomerization. **3o** also shows C–H···π bonds.

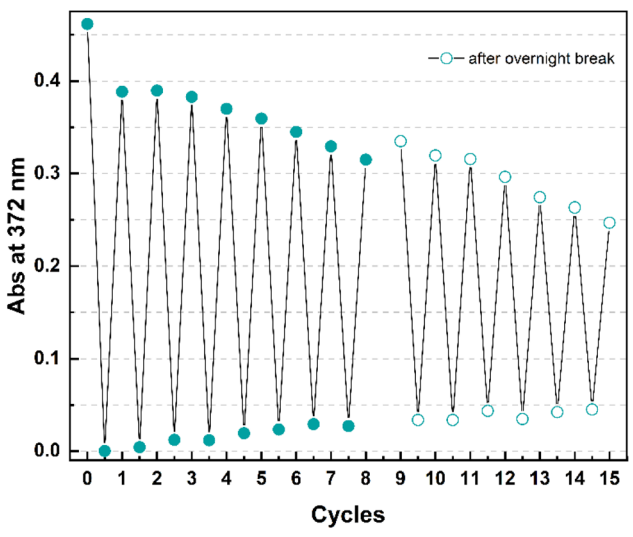

Fig. 8 Cyclability study for **4** in mesitylene showing the absorption change at 372 nm upon 15 irradiation (365 nm, 2 min) – heating (130 °C, 1 h) cycles. After the 8th cycle, the experiment was stopped. A gap is present between cycles 8 and 9 because the overnight break led to some evaporation which required the addition of fresh mesitylene to re-adjust the concentration before the restart of the experiment.

Finally, cyclability experiments were carried out for **4** because of its shortest half-life time within the series. Fifteen irradiation – heating cycles were performed in mesitylene (Fig. 8) by irradiating a solution of **4o** at 365 nm at room temperature for 2 minutes and then by heating it at 130 °C for 1 hour.

After a drop in absorption of around 16% with the first cycle (that can also be partially ascribed to a non-quantitative conversion in 1 h), the following photoisomerization – back-reaction sequences occurred without as significant degradation (*e.g.* 0.08% in cycle 2, 0.5% in cycle 3). As the cycles were carried out manually, the experiment was stopped after eight cycles and continued the following day.

Having observed a slight evaporation of solvent leading to an increase in the absorbance, fresh mesitylene was added in the attempt to re-adjust the concentration to what it was at the end of the 8th cycle before performing the other irradiation-heating sequences. At the end of the experiment, an overall decrease in absorbance of 50% *ca.* was observed.

Conclusions

In summary, five *ortho*-dianthrylbenzenes were synthesized and evaluated for molecular solar thermal (MOST) energy storage. The introduction of electron-donating or -withdrawing substituents on 1,2-di(anthryl)benzene **1o** slightly impacted the optical properties of the switches but significantly influenced the thermal stability of the photogenerated isomers, particularly in the case of difluoro-functionalized **5c** ($t_{1/2}$ = 37 years). The observed storage energy values between around 65 and 94 kJ mol^{-1} and the corresponding energy storage densities (0.14–0.20 MJ kg^{-1}), combined with their solar energy storage efficiencies ranging from 0.38% to 0.66%, make these photoswitches potentially suitable for MOST applications and open the door towards future developments on anthracene-based photochromes in this field. Next, these di(anthryl)benzenes will be further investigated to boost their Φo–c (which appears as the main factor to be improved to achieve better MOST properties), evaluate the impact of the linker ring-size, and achieve on-demand energy release, for example through application of external stimuli different from temperature.

Data availability

The data supporting this article have been included as part of the ESI.†

Author contributions

N. B. performed the synthesis of the investigated switches and their preliminary characterization by UV-vis spectroscopy. L. M. M. completed the characterization of the photoswitches by determining their isomerization quantum yields, by carrying out the kinetics studies, the DSC and NMR experiments to study their back-conversion and the cyclability

experiment. N. B. and J. L. E. performed the real solar conversion experiment to investigate the isomerization under unfiltered sunlight. Z. L. and J. L. E. carried out the computational modelling of the systems and their properties. J. L. E. calculated the solar energy storage efficiencies. K. V. M. supervised the computational part of the project. P. B. and N. B. measured the fluorescence quantum yields. E. M. solved the single crystal structures. N. B. and K. M. P. designed the project. K. M. P. supervised the project and was responsible for funding acquisition. N. B. prepared the original draft. All the authors contributed to the review and editing of the original draft.

Conflicts of interest

There are no conflicts to declare.

Acknowledgements

Funding from the European Commission (H2020-FETPROACT-2019-951801; Molecular Solar Thermal Energy Storage Systems) and the European Research Council (ERC) under grant agreement CoG, PHOTHERM– 101002131 is acknowledged by the authors. The authors would like to also acknowledge the financial support from the Göran Gustafsson Foundation, the Swedish Research Council, the Spanish Ministry for Science and Innovation (project LIPCES, PID2021-123873NB-I00) and the Catalan Institute of Advanced Studies (ICREA). K. V. M. acknowledges the Danish Council for Independent Research, DFF-0136-00081B, DFF-10.46540/3103-00261B and the European Union's Horizon 2020 Framework Programme under grant agreement number 951801 for financial support. E. M. acknowledges financial support from the State Investigation Agency (PID2021-124572OB-C32), and through the Severo Ochoa Programme for Centres of Excellence in R&D (CEX2023-001263-S).

Notes and references

1 T. J. Kucharski, Y. C. Tian, S. Akbulatov and R. Boulatov, *Energy Environ. Sci.*, 2011, **4**, 4449–4472.
2 A. Lennartson, A. Roffey and K. Moth-Poulsen, *Tetrahedron Lett.*, 2015, **56**, 1457–1465.
3 C. Sun, C. Wang and R. Boulatov, *ChemPhotoChem*, 2019, **3**, 268–283.
4 Z. Wang, P. Erhart, T. Li, Z.-Y. Zhang, D. Sampedro, Z. Hu, H. A. Wegner, O. Brummel, J. Libuda, M. B. Nielsen and K. Moth-Poulsen, *Joule*, 2021, **5**, 3116–3136.
5 Q. Qiu, Y. Shi and G. G. D. Han, *J. Mater. Chem. C*, 2021, **9**, 11444–11463.
6 Q. Qiu, S. Yang, M. A. Gerkman, H. Fu, I. Aprahamian and G. G. D. Han, *J. Am. Chem. Soc.*, 2022, **144**, 12627–12631.
7 Z. Wang, H. Hölzel and K. Moth-Poulsen, *Chem. Soc. Rev.*, 2022, **51**, 7313–7326.
8 Q. Qiu, Q. Qi, J. Usuba, K. Lee, I. Aprahamian and G. G. D. Han, *Chem. Sci.*, 2023, **14**, 11359–11364.
9 X. Li, S. Cho, J. Wan and G. G. D. Han, *Chem*, 2023, **9**, 2378–2389.
10 S. Cho, J. Usuba, S. Chakraborty, X. Li and G. G. D. Han, *Chem*, 2023, **9**, 3159–3171.
11 R. J. Salthouse and K. Moth-Poulsen, *J. Mater. Chem. A*, 2024, **12**, 3180–3208.
12 J. Usuba and G. G. D. Han, *Trends Chem.*, 2023, **5**, 577–580.
13 L. Dong, Y. Feng, L. Wang and W. Feng, *Chem. Soc. Rev.*, 2018, **47**, 7339–7368.
14 D. Dong and T. Li, *ChemPhotoChem*, 2024, e202400007.
15 V. A. Bren', A. D. Dubonosov, V. I. Minkin and V. A. Chernoivanov, *Russ. Chem. Rev.*, 1991, **60**, 451–469.
16 J. Orrego-Hernández, A. Dreos and K. Moth-Poulsen, *Acc. Chem. Res.*, 2020, **53**, 1478–1487.
17 Z. Wang, J. Udmark, K. Börjesson, R. Rodrigues, A. Roffey, M. Abrahamsson, M. B. Nielsen and K. Moth-Poulsen, *ChemSusChem*, 2017, **10**, 3049–3055.
18 M. Brøndsted Nielsen, N. Ree, K. V. Mikkelsen and M. Cacciarini, *Russ. Chem. Rev.*, 2020, **89**, 573–586.
19 C. Schøttler, S. K. Vegge, M. Cacciarini and M. B. Nielsen, *ChemPhotoChem*, 2022, **6**, e202200037.
20 K. Moth-Poulsen, D. Ćoso, K. Börjesson, N. Vinokurov, S. K. Meier, A. Majumdar, K. P. C. Vollhardt and R. A. Segalman, *Energy Environ. Sci.*, 2012, **5**, 8534–8537.
21 Z. Yoshida, *J. Photochem.*, 1985, **29**, 27–40.
22 M. O'Donnell, *Nature*, 1968, **218**, 460–461.
23 W. R. Bergmark, G. Jones, T. E. Reinhardt and A. M. Halpern, *J. Am. Chem. Soc.*, 1978, **100**, 6665–6673.
24 H.-D. Becker, *Chem. Rev.*, 1993, **93**, 145–172.
25 H. Bouas-Laurent, J.-P. Desvergne, A. Castellan and R. Lapouyade, *Chem. Soc. Rev.*, 2000, **29**, 43–55.
26 H. Bouas-Laurent, J.-P. Desvergne, A. Castellan and R. Lapouyade, *Chem. Soc. Rev.*, 2001, **30**, 248–263.
27 R. R. Islangulov and F. N. Castellano, *Angew. Chem., Int. Ed.*, 2006, **45**, 5957–5959.
28 G. Ganguly, M. Sultana and A. Paul, *J. Phys. Chem. Lett.*, 2018, **9**, 328–334.
29 S. Chakraborty, H. P. Q. Nguyen, J. Usuba, J. Y. Choi, Z. Sun, C. Raju, G. Sigelmann, Q. Qiu, S. Cho, S. M. Tenney, K. E. Shulenberger, K. Schmidt-Rohr, J. Park and G. G. D. Han, *Chem*, 2024, DOI: 10.1016/j.chempr.2024.06.033.
30 N. Sugiyama, M. Iwata, M. Yoshioka, K. Yamada and H. Aoyama, *Bull. Chem. Soc. Jpn.*, 1969, **42**, 1377–1379.
31 N. C. Yang, D. M. Shold and B. Kim, *J. Am. Chem. Soc.*, 1976, **98**, 6587–6596.
32 I. Zouev, D.-K. Cao, T. V. Sreevidya, M. Telzhensky, M. Botoshansky and M. Kaftory, *CrystEngComm*, 2011, **13**, 4376–4381.
33 Y. Hino, T. Matsuo and S. Hayashi, *ChemPlusChem*, 2022, **87**, e202200157.
34 S. Kataoka, D. Kitagawa, H. Sotome, S. Ito, H. Miyasaka, C. J. Bardeen and S. Kobatake, *Chem. Sci.*, 2024, DOI: 10.1039/D4SC03060E.
35 J. T. Goldbach, T. P. Russell and J. Penelle, *Macromolecules*, 2002, **35**, 4271–4276.
36 J. Van Damme, L. Vlaminck, G. Van Assche, B. Van Mele, O. van den Berg and F. Du Prez, *Tetrahedron*, 2016, **72**, 4303–4311.

37 D. Han, H. Lu, W. Li, Y. Li and S. Feng, *RSC Adv.*, 2017, **7**, 56489–56495.
38 Y. Li, M. Goswami, Y. Zhang, T. Liu, J. Zhang, M. R. Kessler, L. Wang and O. Rios, *Sci. Rep.*, 2020, **10**, 20214.
39 G. Kahraman, B. Durçak, N. Arsu, E. Hey-Hawkins and T. Eren, *Eur. Polym. J.*, 2023, **189**, 111946.
40 D. E. Applequist, M. A. Lintner and R. Searle, *J. Org. Chem.*, 1968, **33**, 254–259.
41 G. Jones, T. E. Reinhardt and W. R. Bergmark, *Sol. Energy*, 1978, **20**, 241–248.
42 T. Nishiuchi, S. Uno, Y. Hirao and T. Kubo, *J. Org. Chem.*, 2016, **81**, 2106–2112.
43 M. Yoshizawa and L. Catti, *Acc. Chem. Res.*, 2019, **52**, 2392–2404.
44 T. Nishiuchi, H. Sotome, K. Shimizu, H. Miyasaka and T. Kubo, *Chem.–Eur. J.*, 2022, **28**, e202104245.
45 T. Nishiuchi, S. Takeuchi, Y. Makihara, R. Kimura, S. Saito, H. Sato and T. Kubo, *Bull. Chem. Soc. Jpn.*, 2022, **95**, 1591–1599.
46 I. Yamazaki, N. Aratani, S. Akimoto, T. Yamazaki and A. Osuka, *J. Am. Chem. Soc.*, 2003, **125**, 7192–7193.
47 L. Catti, N. Kishida, T. Kai, M. Akita and M. Yoshizawa, *Nat. Commun.*, 2019, **10**, 1948.
48 W. Sun, Z. Shangguan, X. Zhang, T. Dang, Z.-Y. Zhang and T. Li, *ChemSusChem*, 2023, **16**, e202300582.
49 Z. Wang, H. Hölzel, L. Fernandez, A. S. Aslam, P. Baronas, J. Orrego-Hernández, S. Ghasemi, M. Campoy-Quiles and K. Moth-Poulsen, Hybrid solar energy device for simultaneous electric power generation and molecular solar thermal energy storage, *Joule*, 2024, DOI: **10.1016/j.joule.2024.06.012**.
50 C. Bannwarth, S. Ehlert and S. Grimme, *J. Chem. Theory Comput.*, 2019, **15**, 1652–1671.
51 S. Grimme, A. Hansen, S. Ehlert and J.-M. Mewes, *J. Chem. Phys.*, 2021, **154**, 064103.
52 A. Najibi and L. Goerigk, *J. Chem. Theory Comput.*, 2018, **14**, 5725–5738.
53 G. Henkelman, B. P. Uberuaga and H. Jónsson, *J. Chem. Phys.*, 2000, **113**, 9901–9904.
54 C. Bannwarth, E. Caldeweyher, S. Ehlert, A. Hansen, P. Pracht, J. Seibert, S. Spicher and S. Grimme, *Wiley Interdiscip. Rev.: Comput. Mol. Sci.*, 2021, **11**, e1493.
55 F. Neese, *Wiley Interdiscip. Rev.: Comput. Mol. Sci.*, 2012, **2**, 73–78.
56 J. L. Elholm, A. E. Hillers-Bendtsen, H. Hölzel, K. Moth-Poulsen and K. V. Mikkelsen, *Phys. Chem. Chem. Phys.*, 2022, **24**, 28956–28964.
57 J. L. Elholm, Z. Liasi, M. K. Mikkelsen, A. E. Hillers-Bendtsen and K. V. Mikkelsen, *Phys. Chem. Chem. Phys.*, 2023, **25**, 21964–21969.
58 A. E. Hillers-Bendtsen, J. L. Elholm, O. B. Obel, H. Hölzel, K. Moth-Poulsen and K. V. Mikkelsen, *Angew. Chem., Int. Ed.*, 2023, **62**, e202309543.

